Designing Interfacial Reactions for Nanometer-Scale Surface Patterning of PDMS with Controlled Elastic Modulus

Laura O. Williams,[1] Emmanuel K. Nava,[1] Anni Shi,[1] Tyler J. Roberts,[2] Chelsea S. Davis,[3] and Shelley A. Claridge[1,4,*]

[1]Department of Chemistry, Purdue University, West Lafayette, Indiana 47907
[2]Davidson School of Chemical Engineering, Purdue University, West Lafayette, Indiana 47907
[3]School of Materials Engineering, Purdue University, West Lafayette, Indiana 47907
[4]Weldon School of Biomedical Engineering, Purdue University, West Lafayette, Indiana 47907
Address correspondence to: claridge@purdue.edu, (phone) 765-494-6070

ABSTRACT: Control over the surface chemistry of elastomers such as polydimethylsiloxane (PDMS) is important for many applications. However, achieving nanostructured chemical control on amorphous material interfaces below the length scale of substrate heterogeneity is not straightforward, and can be particularly difficult to decouple from changes in network structure that are required for certain applications (*e.g.* variation of elastic modulus for cell culture). We have recently reported a new method for precisely structured surface functionalization of PDMS and other soft materials, which displays high densities of ligands directly on the material surface, maximizing steric accessibility. Here, we systematically examine structural factors in the PDMS components (*e.g.* base and crosslinker structures) that impact efficiency of the interfacial reaction that leads to surface functionalization. Applying this understanding, we demonstrate routes for generating equivalent nanometer-scale functional patterns on PDMS with elastic moduli from 0.013 to 1.4 MPa, establishing a foundation for use in applications such as cell culture.

KEYWORDS: PDMS, monolayer, elastic modulus, polydiacetylene, surface chemistry, chemical patterning

INTRODUCTION

A broad range of materials applications make use of soft, amorphous polymers including polydimethylsiloxane (PDMS) and hydrogels.[1-3] In many cases, it is useful to control their surface chemistry.[4-5] In some cases, it is also desirable to control surface chemistry independent of mechanical properties; for instance, in PDMS-based wearable electronics, soft blends are necessary to achieve conformal contact with human skin.[6] Moreover, in elastomeric and hydrogel materials for cell culture, ligand presentation and substrate modulus are both known to impact cell adhesion and differentiation,[7-8] raising the importance of precise display of fuctional group clusters at the soft material surface, with elastic moduli chosen to match tissue-specific mechanical properties.

Nanoscale control over polymer film structure has been a problem of long-standing interest. Nanoscale phase separation has been demonstrated using several block copolymers, relying on chemical differences between polymer blocks to drive phase separation[9-10] at sub-100-nm scales. Nanometer-scale surface topography replication has also been achieved for certain classes of relatively hard polymers (*e.g.* PMMA, highly crosslinked D_4^H/D_4^V PDMS),[11] and can be used in conjunction with chemical patterning strategies to in some cases generate chemical features at scales as small as 20 nm.[12] However, precise nanoscale control over surface chemical patterning of soft materials remains a significant challenge, particularly in conjunction with elastic modulus tuning in the range suitable for soft tissue; in part this is due to nano-to-microscale heterogeneities in bulk polymeric materials with larger mesh sizes.

Recently, we have demonstrated that it is possible to generate nm-scale chemical patterns in the surface chemistry of PDMS[13-16] and other soft materials.[17-18] Functionalization starts by assembling striped phases of diacetylene (DA)-modified amphiphiles on highly oriented pyrolytic graphite (HOPG). In the striped phases, the alkyl chain of the amphiphile lies flat on the HOPG substrate (Figure 1a), generating 1-nm-wide stripes of paired functional headgroups embedded in a stripe of exposed alkyl chains.[19-23] Photopolymerization of aligned DA groups (Figure 1a, bottom), produces polydiacetylene (PDA) backbones that tether together molecules within the layer. If PDMS is then cured on top of the striped PDA (sPDA) layer (Figure 1a, center), the hydrosilylation reaction between vinyl-terminated PDMS base polymer and silane groups in the crosslinker, in the presence of a transition metal catalyst, also forms covalent linkages to the PDA backbone.[13] As a result, when the PDMS is exfoliated from the HOPG, the sPDA monolayer can be removed with it, producing an extremely high-resolution surface functionalization layer (Figure 1a, right).

Understanding the relationship between PDMS network structure and the interfacial reaction efficiency would potentially make it possible to control surface functionalization density independent of elastic modulus. However, interfacial reactions are frequently challenging to characterize, and can be 2–3 orders of magnitude less efficient than similar reactions in bulk (e.g. hydrolysis of N-hydroxysuccinimide esters embedded in alkanethiol monolayer vs in solution, or hydrolysis of polystyrene-block-poly(tert-butylacrylate) thin films),[24-25] although there are also cases in which interfacial

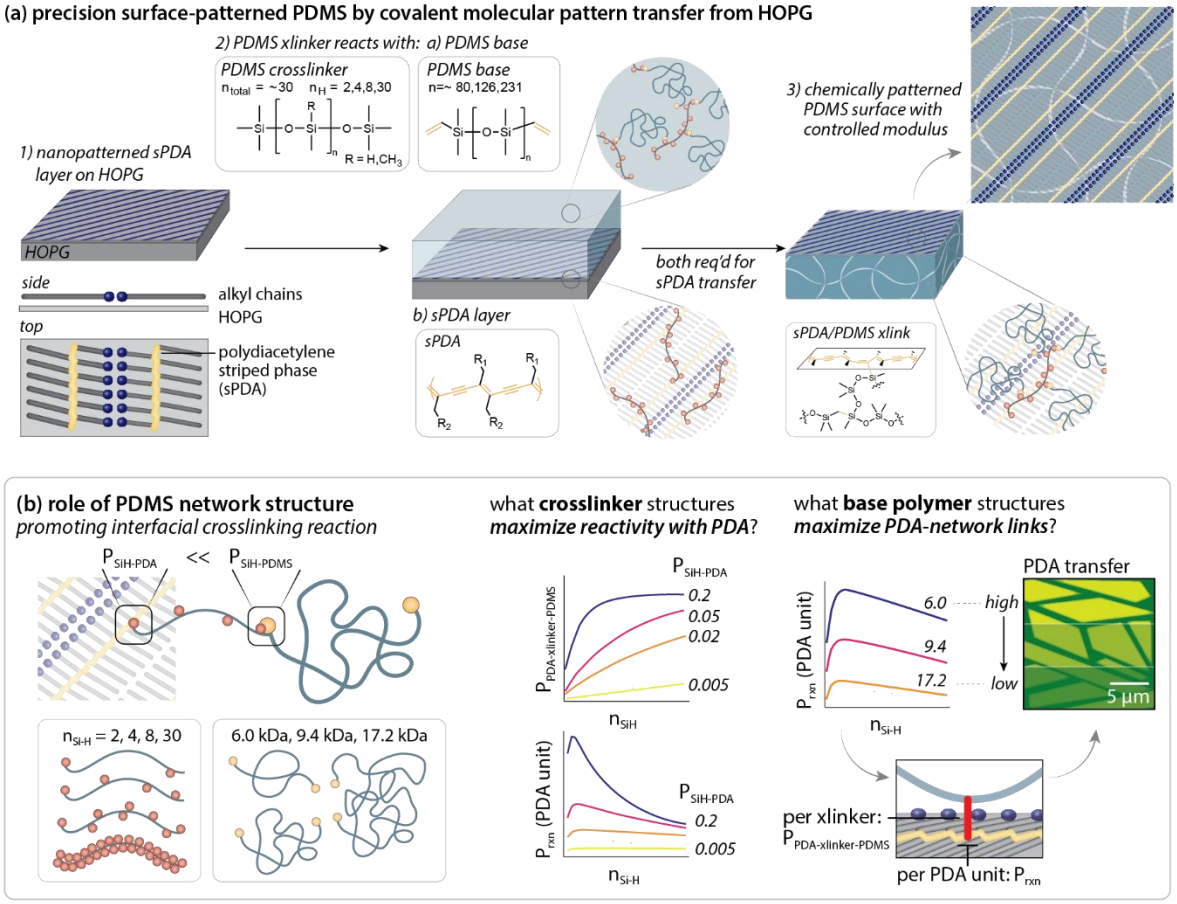

Figure 1. (a) Illustration of striped phase assembly on HOPG and transfer of sPDAs to PDMS for nanometer-scale functional patterning. (b) Illustration of PDMS base and crosslinker structure, and potential impacts on crosslinking reaction efficiency.

reactions can have similar efficiency to the bulk reaction (*e.g.* hydrolysis of poly(solketal methacrylate) to poly(glycerol methacrylate)),[26-27] highlighting the importance of systematic control. Our sPDA transfer reaction exemplifies these challenges — although it is possible to observe the extent of transfer based on fluorescence emission from the PDA, it is not straightforward to directly observe the crosslinking process that leads to transfer. Recently, we have begun to develop an understanding of the the relationship between PDA length and transfer efficiency, which suggests the likelihood that only 1-2% of the PDA units in each sPDA undergo crosslinking, when carried out with Sylgard-184, a commercial PDMS formulation.[14,16]

Although PDMS formulations such as Sylgard-184 are very broadly used in micro- and nanostructured materials applications,[1-3] formulations (including base and crosslinker structures) are proprietary, and can further comprise a range of components beyond the base and crosslinker. For instance, the Sylgard-184 'base' component can contain >30% dimethylvinylated and trimethylated surface-functionalized silica filler particles[28] that form branched, chainlike aggregates,[29] providing reinforcement to the PDMS network. Thus, it is not straightforward to directly modify Sylgard blend composition in ways that illuminate the relationship between PDMS network structure and interfacial reaction efficiency.

Here, we design custom PDMS formulations that enable us to control base and crosslinker structure, and by extension the concentration of reactive groups and their distribution within the PDMS (Figure 1b, left). We develop models predicting the interfacial reaction efficiency in relation to PDMS crosslinker and base structure (Figure 1b, right). Then, combining molecular- and micro-scale data on the monolayer transfer in relation to PDMS formulation, we develop stiff and soft formulations of PDMS that produce high surface functionalization efficiency relative to Sylgard-184. This provides an important first step toward materials for applications such as cell culture, where historically it has been difficult to deconvolve functionalization density from substrate mechanical properties.

RESULTS AND DISCUSSION

Preparation of striped polydiacetylene (sPDA) monolayers and transfer to PDMS. To functionalize PDMS surfaces, sPDA monolayers of 10,12-tricosadiynoic acid (TCDA) were first prepared via Langmuir–Schaefer (LS) conversion.[1,2] Molecules in striped phases self-assemble in epitaxy with the underlying HOPG lattice,[30-31] producing lamellar assemblies consisting of alternating rows of ~1 nm stripes of polar headgroups and ~5 nm stripes of exposed alkyl chains (Figure 2a). UV irradiation induces topochemical polymerization, in which adjacent diacetylene (DA) groups are converted into sPDAs. The resulting PDA backbones (highlighted in gold in Figure 2a, bottom) tether together molecules along each row, stabilizing the monolayer for eventual transfer to PDMS. Energy-minimized molecular models of the unpolymerized striped phase illustrate edge-to-edge distances of 6.1 nm, in good agreement with the lamellar

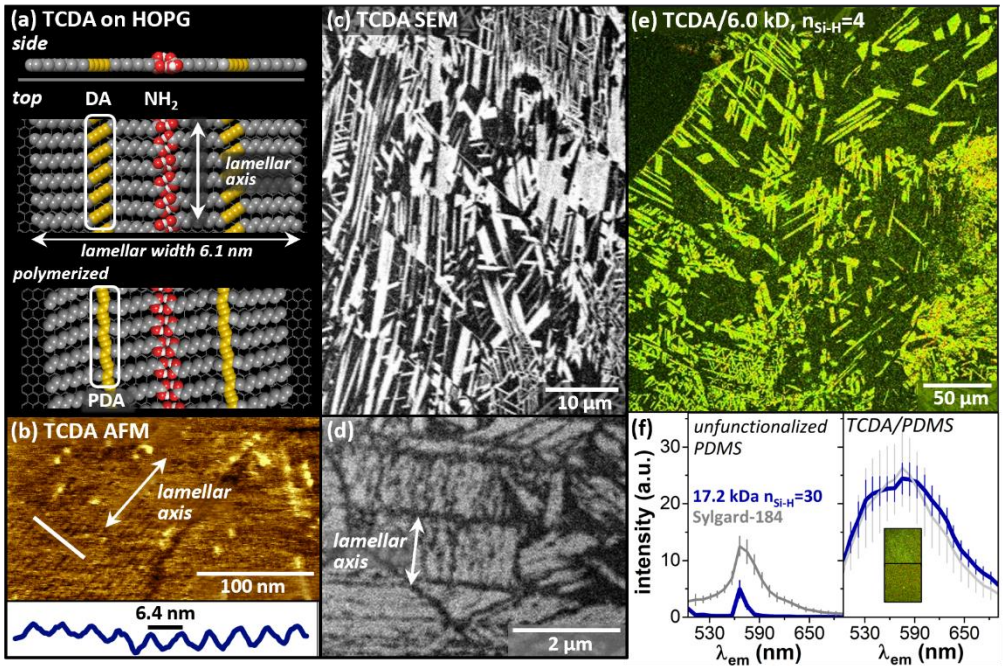

Figure 2. (a) Molecular model of amphiphile assembly and polymerization on HOPG. (b) AFM image of TCDA striped phase monolayer on HOPG. (c,d) SEM images of TCDA monolayer on HOPG illustrating (c) domain structure and (d) lamellar axes. (e)Fluorescence micrograph of TCDA transferred to custom PDMS blend. (f) Fluorescence emission spectra of unfunctionalized (left) and functionalized (right) PDMS.

periodicity of 6.4 nm observed in AFM images (Figure 2b). SEM imaging reveals long-range ordering (Figure 2c,d) with domain edge lengths of >10 µm[3,4] achieved routinely. Here, we have chosen a monolayer with significant vacancies (darker regions) between ordered domains (brighter regions) that form with hexagonal symmetry reflecting the symmetry of the underlying HOPG substrate, to facilitate visual interpretation of domain structure. However, it is also straightforward to prepare surfaces with essentially complete monolayer coverage, which was done for quantification experiments described in the manuscript (see Figure S4 for examples).

Previously, we have shown that sPDAs can be covalently transferred to the surface of commercially-available Sylgard-184 PDMS (Figure 1a, center and right) by mixing the two components of the PDMS blend (base and curing agent), pouring the liquid PDMS mixture onto the sPDA/HOPG surface, curing the PDMS, then gently exfoliating the cured PDMS from the HOPG.[13-14,16] Although the constrained blue-form PDA initially synthesized on the hard HOPG substrate is non-emissive, transfer to the softer PDMS substrate enables relaxation to the twisted red-form PDA,[13] which is weakly fluorescent, with a polarized free exciton ^1B_u transition.[32] We have previously demonstrated that fluorescence emission from the sPDA backbone can be used both to visualize surface functionalization, and to quantify the relative extent of sPDA transfer (and hence the relative surface density of functional groups in different regions of the surface).[14,16] We have shown that transfer efficiency varies with polymer length,[16] with average sPDA lengths of 100–200 repeat units (50–100 nm) required for efficient transfer, and models suggesting that 2–3 covalent linkages are required per sPDA for transfer.

Here, we developed a series of custom PDMS blends that provided transfer characteristics comparable to those of the Sylgard-184, but were comprised of known components. As a starting point, we generated stoichiometric blends (Figure 1b, left) consisting of a vinyl-terminated base polymer with a specified molecular weight (6.0, 9.4, or 17.2 kDa), and a 2.0 kDa crosslinker containing an average of 2, 4, 8, or 30 reactive Si-H groups per chain (n_{Si-H} = 2, 4, 8, 30). See the Experimental Methods in the Supporting Information for product numbers and formulation details. The Karstedt catalyst (platinum-divinyltetramethyldisiloxane complex, 2% Pt in xylene) is widely used in PDMS crosslinking,[33] and was utilized in all of our blends; 1,3,5,7-tetravinyl-1,3,5,7-tetramethylcyclotetra-siloxane was selected as a moderator to slow crosslinking.

Fluorescence emission was used to visualize and quantify transfer to PDMS. See the Supporting Information for detailed experimental methods, and for data analysis of confocal fluorescence micrographs. The image in Figure 2e was acquired using the blend comprised of 6.0 kDa base and n_{Si-H} = 4 crosslinker, cured in contact with a TCDA sPDA layer on HOPG and subsequently exfoliated to create a carboxylic acid-functionalized surface; here again, a monolayer with partial coverage was chosen to highlight molecular domain structure. As observed previously with Sylgard-184, hexagonally-oriented fluorescent regions are visible on the PDMS surface, with morphologies similar to those observed in microscale SEM images of TCDA domains on HOPG (Figure 2c,d). Comparing emission spectra, we noted differences in the background fluorescence of Sylgard-184 and custom blends (Figure 2f, left). Overall, lower fluorescence was associated with the custom blends, potentially related to the absence of fillers. When respective background spectra for unfunctionalized PDMS blends were subtracted, the remaining sPDA spectral emission shape was similar for samples of custom and commercial PDMS (Figure 2f, right).

Variation of PDMS base polymer and crosslinker structure to control interfacial reaction. To understand the factors that

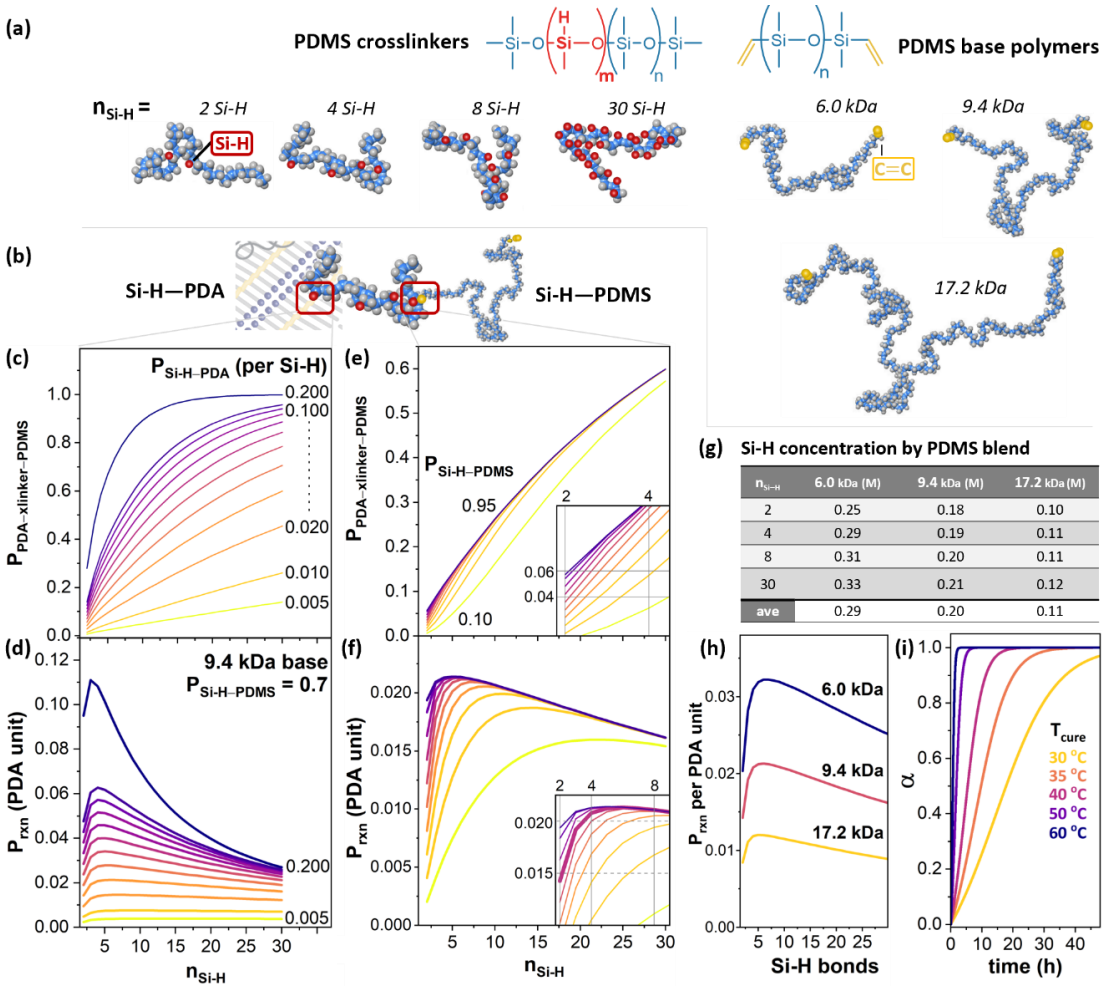

n_{Si-H}	6.0 kDa (M)	9.4 kDa (M)	17.2 kDa (M)
2	0.25	0.18	0.10
4	0.29	0.19	0.11
8	0.31	0.20	0.11
30	0.33	0.21	0.12
ave	0.29	0.20	0.11

Figure 3. (a) Molecular models of PDMS crosslinkers (2.0 kDa, n_{Si-H} = 2, 4, 8, and 30) and base polymers (6.0 kDa, 9.4 kDa, and 17.2 kDa) used in this study. Note crosslinkers are shown at somewhat larger scale than PDMS base molecules, to enhance visibility of Si-H groups (red circles). (b) Schematic illustrating two elements of the reaction network examined in calculations here: Si-H–PDA linkage (left) and Si-H–PDMS linkage (right). (c) $P_{PDA-xlinker-PDMS}$ for crosslinkers with varying n_{Si-H}, for per-site reaction probabilities of 0.005 to 0.200. (d) P_{rxn} per PDA unit, for the 9.4 kDa base, $P_{Si-H-PDMS}$ = 0.7, and the range of $P_{Si-H-PDA}$ values shown in (c). (e) $P_{PDA-xlinker-PDMS}$ for crosslinkers with varying n_{Si-H}, for per-site reaction probabilities of 0.03 and $P_{Si-H-PDMS}$ = 0.10 to 0.95. (f) P_{rxn} per PDA unit, for the 9.4 kDa base, $P_{Si-H-PDA}$ = 0.03, and the range of $P_{Si-H-PDMS}$ values shown in (e). (g) Si-H concentration for each PDMS blend. (h) P_{rxn} for each of the three base molecular weights tested, with $P_{Si-H-PDA}$ = 0.03. (i) Modeled PDMS curing times vs temperature.

influence the interfacial crosslinking reaction that leads to sPDA transfer, we generated models predicting the impacts of crosslinker (Figure 3a, left) and base (Figure 3a, right) structure. See the Supporting Information for more details on calculations described throughout this section. To participate in PDA exfoliation, a crosslinker molecule must have one Si-H bond react with the PDA (Figure 3b, left), and another react with a PDMS base molecule (Figure 3b, right), ultimately linking to the larger PDMS mesh. Crosslinkers with larger numbers of Si-H bonds (red circles in model) should have a greater probability of forming both linkages and participating in PDA exfoliation. However, to maintain stoichiometric balance of Si-H and vinyl groups, smaller numbers of such crosslinker molecules are used in our blends, potentially offsetting this trend for larger values of n_{Si-H}.

We first examined probabilities of Si-H—PDA bond formation, expected to be the limiting step in transfer. While it is not known whether the Si-H—PDA and Si-H—PDMS reactions would be equivalent in terms of bulk reaction kinetics, overall similarities in the reactions led us to use this guideline for initial parameterization of the system. Figure 3c shows calculated probabilities of a crosslinker successfully joining a PDA to the PDMS mesh ($P_{PDA-xlinker-PDMS}$), varying the probabilities of Si-H–PDA crosslinking per Si-H group ($P_{Si-H-PDA}$) from 0.005 to 0.20, and varying the number of Si-H groups per molecule (n_{Si-H}) from 2 to 30. Details of these calculations are described in the Supporting Information; overall, the probabilities are related using the following equation:

$$P_{PDA-xlinker-PDMS} = 1 - (1 - P_{SiH-PDA})^{n_{Si-H}} - (1 - P_{SiH-PDMS})^{n_{Si-H}} + (1 - P_{SiH-PDA} - P_{SiH-PDMS})^{n_{Si-H}} \quad (1)$$

At the lowest values of $P_{Si-H-PDA}$ (yellow and orange traces), even the most reactive crosslinkers (n_{Si-H} = 30) have a low probability of reacting with a PDA to facilitate transfer. Conversely, at the highest values of $P_{Si-H-PDA}$ (blue and violet traces), even the less reactive crosslinkers (including n_{Si-H} = 4, 8) produce significant crosslinking probabilities. For all values

of $P_{Si\text{-}H\text{–}PDA}$ tested, the probability of crosslinking remains low for the least reactive crosslinker ($n_{Si\text{-}H}$ = 2).

We then used these values to calculate the probability of a successful crosslinking reaction *per PDA repeat unit* in the monolayer (Figure 1b, bottom right). Previously we have used this parameter (P_{rxn}) in modeling the extent of monolayer transfer, based on modifications of PDA length.[16] Here, P_{rxn} changes with PDMS blend structure in two ways. (1) P_{rxn} is proportional to $P_{PDA\text{-}xlinker\text{-}PDMS}$, the crosslinking probability *per crosslinker molecule*, which increases for larger values of $n_{Si\text{-}H}$. (2) P_{rxn} is proportional to the number of crosslinker molecules present in the few nm of PDMS closest to the PDA monolayer, which *decreases* for larger values of $n_{Si\text{-}H}$, as described previously. Figure 3d shows P_{rxn}, for $P_{Si\text{-}H\text{–}PDA}$ =0.005–0.200 (yellow trace = 0.005; blue trace = 0.200). Overall, these models predict that transfer should be substantially more efficient for crosslinkers with intermediate numbers of reactive Si-H groups (including $n_{Si\text{-}H}$ = 4, 8) and least efficient for $n_{Si\text{-}H}$ = 2. The difference in efficiency becomes greater at higher values of $P_{Si\text{-}H\text{–}PDA}$. Overall, probabilities in the range of 0.03 provide P_{rxn} values from 0.015–0.020, which would be in line with our previous estimates for Sylgard-184.

The models in Figure 3d use a value of 0.700 for the probability of Si-H–PDMS crosslinking at each reactive site ($P_{Si\text{-}H\text{–}PDMS}$). This was chosen to allow a large range of tested values for $P_{Si\text{-}H\text{–}PDA}$. Figure 3e re-examines reaction efficiency using $P_{Si\text{-}H\text{–}PDA}$ = 0.03 and varying $P_{Si\text{-}H\text{–}PDMS}$ from 0.10 to 0.95. Overall, calculated values differ most significantly for low $n_{Si\text{-}H}$ (Figure 3e, inset), which is reasonable — at high $n_{Si\text{-}H}$ (many Si-H groups per crosslinker), crosslinking to the PDMS network becomes very likely, even for relatively low values of $P_{Si\text{-}H\text{–}PDMS}$.

Calculating values of P_{rxn} (Figure 3f) for the Si-H–PDMS crosslinking probabilities shown in Figure 3e, changes in Si-H–PDMS crosslinking mostly impact the difference in predicted transfer for $n_{Si\text{-}H}$ = 2 and $n_{Si\text{-}H}$ = 4, with very high crosslinking efficiencies minimizing the difference in transfer (Figure 3f, inset). At the lowest Si-H–PDMS reaction efficiencies (yellow trace), higher values of $n_{Si\text{-}H}$ are required for PDA transfer; however, such low PDMS crosslinking efficiencies would also impact formation of the bulk mesh, and are not expected in the experiments here.

Finally, we examined how changes in PDMS blend structure may impact reaction probability. For the blends used here, shorter base polymers resulted in higher concentrations of both vinyl and Si-H reactive groups (Figure 3g), ~0.3 M for the 6.0 kDa base, and ~0.1 M for the 17.2 kDa base. Thus, calculated P_{rxn} values (Figure 3h) were higher for the 6.0 kDa base polymer (blue trace) than for the 17.2 kDa base (gold trace), by a factor of approximately 3.

To select a curing schedule, we utilized the Kamal model[34] to approximate PDMS network formation (α) *vs* time at a range of possible curing temperatures (Figure 3i, see Experimental Methods for details). Because PDAs can undergo thermal side reactions at temperatures near 60 °C, we selected a lower temperature (38 °C) this leads to a relatively long curing time (>24 h to reach full conversion). To minimize possible variability in extent of conversion between different reactions, we utilized a curing time of 39 h.

Transfer with variation of crosslinker structure. Next, we began to experimentally examine sPDA transfer with varying crosslinker composition. Experimentally, when we test the 9.4 kDa base with all four crosslinkers (Figure 4a), we observe differences in fluorescence emission (Figure 4b,c), with a lower values for $n_{Si\text{-}H}$ =2 than for the other crosslinkers tested (Figure 4d, final row of table). When we compared these with modeled values of P_{rxn} from Figure 3 for $n_{Si\text{-}H}$ = 2,4,8, and 30, and for values of $P_{Si\text{-}H\text{–}PDA}$, from 5–0.5%, all of these produce ratios of $P_{n=4}/P_{n=2}$ ~ 1.5 (similar to 1.65 observed experimentally) and $P_{n=4}/P_{n=8}$ ~ 1.0 (similar to 1.02 observed experimentally). However, higher crosslinking probabilities produce larger ratios of $P_{n=4}/P_{n=30}$ (as high as 1.76) while a value of 0.95 was observed experimentally, likely consistent with relatively low Si-H–PDA crosslinking probabilities (0.5–2%). We note that the experimentally observed $P_{n=4}/P_{n=2}$ is slightly higher than predicted values with $P_{Si\text{-}H\text{–}PDMS}$ = 0.7; this would be consistent with the modest overprediction of successful PDA–xlinker–

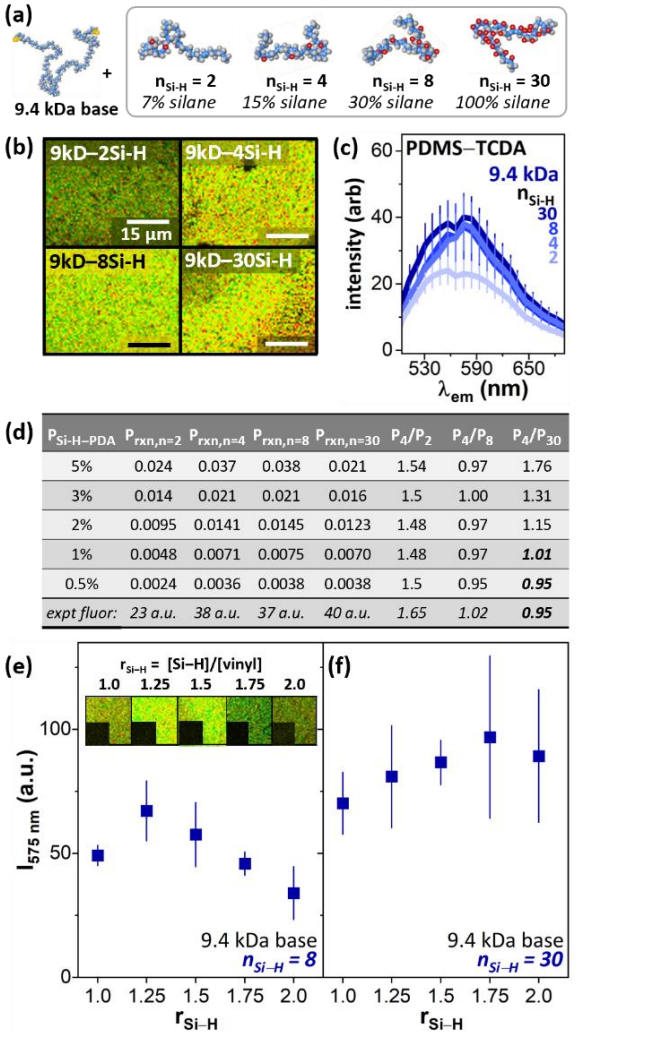

$P_{Si\text{-}H\text{–}PDA}$	$P_{rxn,n=2}$	$P_{rxn,n=4}$	$P_{rxn,n=8}$	$P_{rxn,n=30}$	P_4/P_2	P_4/P_8	P_4/P_{30}
5%	0.024	0.037	0.038	0.021	1.54	0.97	1.76
3%	0.014	0.021	0.021	0.016	1.5	1.00	1.31
2%	0.0095	0.0141	0.0145	0.0123	1.48	0.97	1.15
1%	0.0048	0.0071	0.0075	0.0070	1.48	0.97	***1.01***
0.5%	0.0024	0.0036	0.0038	0.0038	1.5	0.95	***0.95***
expt fluor:	*23 a.u.*	*38 a.u.*	*37 a.u.*	*40 a.u.*	*1.65*	*1.02*	***0.95***

Figure 4. (a) Illustration of base and crosslinkers tested in (b-f). (b,c) Fluorescence (b) micrographs and (c) spectra of 9.4 kDa base with each of the tested crosslinkers. (d) Table of calculated P_{rxn} for $n_{Si\text{-}H}$ = 2,4,8,30, and ratios of crosslinking probabilities; last row compares these values with experimentally observed values. (e,f) Fluorescence emission from nonstoichiometric blends of the 9.4 kDa base with the (e) $n_{Si\text{-}H}$ = 8 crosslinker or (f) $n_{Si\text{-}H}$ = 30 crosslinker. Images in (e) illustrate fluorescence intensity for functionalized PDMS at each $r_{Si\text{-}H}$, with insets illustrating emission from unfunctionalized PDMS.

PDMS bond formation in our models for $n_{Si\text{-}H}$ = 2, as described earlier.

Finally, we examined the impacts of modifying the blend stoichiometry (Figure 4e) to increase the abundance of Si-H bonds in comparison with vinyl groups ($r_{Si\text{-}H}$ = [Si-H]/[vinyl]). Varying $r_{Si\text{-}H}$ from 1.0 to 2.0 produced optimal transfer at $r_{Si\text{-}H}$ = 1.25, consistent with curing data from Meissner and coworkers that found optimal curing at $r_{Si\text{-}H}$ = 1.25 for end-linked PDMS blends that cure via hydrosilylation.[35] Increasing stoichiometry for the $n_{Si\text{-}H}$ = 30 crosslinker (Figure 4f) produced increases across the range tested (up to a 2:1 ratio), which may be consistent with a situation in which not all 30 Si-H groups in a single crosslinker can form linkages, producing a lower effective stoichiometry. Across the range tested, the $n_{Si\text{-}H}$ = 30 crosslinker produced somewhat higher PDA fluorescence emission for transfer experiments, in comparison with $n_{Si\text{-}H}$ = 8 (Figure 4f vs Figure 4e). However, for $n_{Si\text{-}H}$ = 30 blends it was more challenging to ensure even curing, due to the high reactivity of the crosslinker, so we used $n_{Si\text{-}H}$ = 8 blends as standards for comparison in subsequent experiments.

Reformulation of PDMS to achieve surface functionalization with a range of mechanical properties. For many applications (*e.g.* wearable electronics, cell culture), it would be important to control the Young's modulus of elastomers and other soft materials independent of surface functionalization density. Here, we carried out experiments aimed at providing surface functionalization on PDMS formulations with substantial differences in modulus and network structure. In each case, because the local clustering of functional groups (*e.g.* COOH groups in transferred TCDA monolayers) is controlled through the sPDA structure, the overall surface density of functional groups can be independently controlled based on PDMS crosslinker structure.

First, we compared sPDA transfer using stoichiometric PDMS formulations comprised of the $n_{Si\text{-}H}$ = 8 crosslinker and a base with mass of 6.0 kDa, 9.4 kDa, or 17.2 kDa (Figure 5a). Here, shorter base polymers generate a higher concentration of reactive groups in the PDMS blend, and experimentally we observe the highest sPDA fluorescence emission for the 6.0 kDa blend (71 a.u. vs 37 a.u. for the 17.2 kDa blend). In line with expectations, use of the $r_{Si\text{-}H}$ = 1.25 nonstoichiometric blend increased transfer (to 98 a.u. for 6.0 kDa and 46 a.u. for 17.2 kDa). These differences are in reasonable agreement with the values modeled in Figure 3, which predict essentially 2-fold and 3-fold increases in transfer for 9.4 and 6.0 kDa bases in comparison with 17.2 kDa.

One goal in these experiments was to establish conditions that enabled equivalent surface functionalization densities for PDMS formulations with very different elastic moduli. We performed indentation experiments (see Experimental Methods in Supporting Information) to characterize moduli for our custom formulations (Figure 5b). Overall, the 6.0 kDa base produced the greatest differences in mechanical properties, with an observed elastic modulus of 0.013 MPa for the 6.0 kDa/$n_{Si\text{-}H}$=2 formulation, and 1.4 MPa for the 6.0 kDa/$n_{Si\text{-}H}$=8 formulation (similar to 1.7 MPa for Sylgard-184). Thus, we used this pair of formulations in additional testing below.

We know from previous experiments that the hydrophilic headgroups in the sPDA layer adsorb water from the

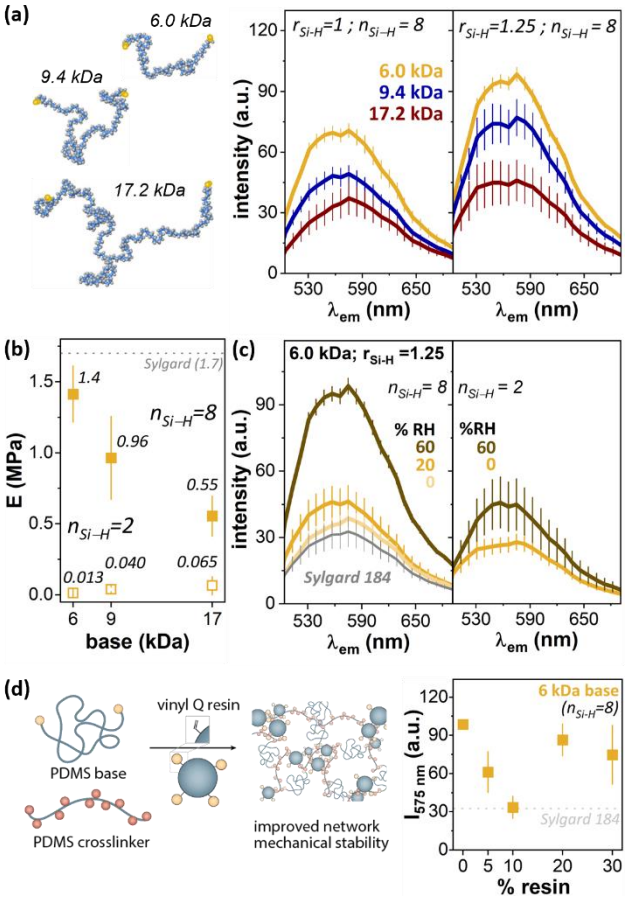

Figure 5. (a) sPDA fluorescence emission spectra of surface-functionalized PDMS blends comprised of $n_{Si\text{-}H}$ = 8 crosslinker and base polymer with mass of 6.0 kDa, 9.4 kDa, or 17.2 kDa, with Si-H:vinyl stoichiometries of 1:1 (left) or 1.25:1 (right). (b) Elastic modulus measurements for each PDMS base with $n_{Si\text{-}H}$ = 8 (filled squares) and $n_{Si\text{-}H}$ = 2 (empty squares). (c) Effects of decreasing environmental humidity for sPDA transfer to 6.0 kDa base cured with $n_{Si\text{-}H}$ = 8 (left) and $n_{Si\text{-}H}$ = 2 (right), compared against sPDA transfer to Sylgard-184 cured at 60% r.h. (grey trace in left panel). (d) Fluorescence emission spectra from surface-functionalized PDMS blends with 6.0 kDa base and $n_{Si\text{-}H}$ = 8 crosslinker, with addition of a silica resin (0–30%).

environment, to an extent dependent upon relative humidity.[36-38] This phenomenon would have the potential to impact local PDMS crosslinking efficiency, for instance by causing unwanted side reactions that produce defects in the mesh. With this in mind, we tested the impacts of controlling environmental humidity as PDMS was applied to sPDA/HOPG substrates (Figure 5c).

Somewhat unexpectedly, decreased environmental humidity (20% and 0% r.h., *vs.* 60% r.h.) was associated with an ~2-fold *decrease* in transfer (from 98 a.u. at 60% r.h. to 46 and 39 a.u., respectively, for 20% r.h. and 0% r.h.). Although there are room temperature vulcanizable (RTV) PDMS blends that are designed to be moisture-curable,[4,39] our custom blends do not contain functional groups typical of RTV moisture-curing (*e.g.* acetoxy, ketoxime, alkoxy), and we did not observe substantial changes in curing of the bulk PDMS at high *vs.* low relative humidity. Thus, this may suggest the additional moisture is primarily impacting the PDA–PDMS crosslinking reaction, providing avenues for future interfacial reaction

design to control transfer. From a practical perspective, this means that transfer is efficient under our typical laboratory atmospheric conditions in summer (50–60% r.h.), but not in winter (10–20% r.h.), and that simple environmental controls (here, a small portable humidifier) substantially improve transfer reproducibility.

Commercial PDMS blends such as Sylgard-184 often include fillers (fumed silica, vinyl resin) to improve mechanical properties such as tear strength and elongation. Here, we tested the impacts of a silica resin additive (Figure 5d). In these tests, blends containing 5–10% resin exhibited decreased transfer, however transfer returned to nearly the levels observed for unfilled blends for mixtures containing 20–30% resin, which is typically described as the optimal range for this filler. Thus, it is possible to prepare both filled and unfilled blends with control over surface functionalization density.

CONCLUSIONS

Here, we have examined structural design principles that lead to more efficient interfacial reactions between monolayers of fully-extended polydiacetylenes and a PDMS network undergoing *in situ* crosslinking. Overall, we find that both the concentration and distribution of reactive silane groups are important predictors of sPDA transfer efficiency, with the outcome that short base polymers (here, 6.0 kDa), intermediate percentages of reactive Si-H groups in the crosslinker (here, n_{Si-H} = 4,8) and slight stoichiometric excess of crosslinkers (r_{Si-H} = 1.25) all increase transfer efficiency.

As expected, metrics of apparent reaction probabilities point to lower reactivity of Si-H groups toward interfacial PDA units in comparison with PDMS vinyl groups. However, the difference in reaction probability appears to be ≤ 2 orders of magnitude. This difference is modest in comparison with other interface-*vs*-bulk reactivity differences studied previously, which is perhaps more surprising given that the PDA would not normally be considered to be as reactive toward hydrosilylation as a terminal vinyl group. One interpretation may be that the PDMS vinyl groups competing with PDA units for Si-H groups are themselves attached to PDMS base molecules localized near the interface and frequently subject to conformational constraints. Conversely, it also appears that the surface-constrained sPDAs are surprisingly competitive substrates for hydrosilylation.

Overall, this may point to more general routes for designing interfacial reaction networks that operate by using an interface to promote reactivity of one reaction partner (e.g. through controlled display geometries or strain), while limiting reactivity of an otherwise more reactive partner through conformational restrictions near the interface.

EXPERIMENTAL METHODS

See Supporting Information for more detailed Experimental Methods.

Materials. See detailed experimental methods in Supporting Information.

Langmuir-Schaefer transfer to generate striped TCDA films. Striped phase 10,12-tricosadiynoic acid (TCDA) films were prepared using a temperature-controlled Langmuir-Schaefer conversion method reported previously,[40-42] and described briefly here. Langmuir-Schaefer transfers were performed on a microTrough XL Langmuir-Blodgett trough (Kibron Inc., Helsinki, Finland) with a customized temperature-controlled magnetic transfer stage reported previously.[43] HOPG substrates were glued to stainless-steel AFM specimen discs. For each transfer, the HOPG on the specimen disc was mounted on the temperature-controlled transfer stage, immediately following HOPG cleavage. The temperature of substrates was maintained at 30 °C to avoid subphase condensation and thermal polymerization of TCDA on HOPG. 34.5 µL of 0.75 mg/mL TCDA in $CHCl_3$ was deposited in evenly distributed 1 µL droplets on a milli-Q water subphase at 30 °C. The system was allowed to equilibrate and to evaporate the $CHCl_3$ carrier solvent for 15 min. Compression of the subphase was carried out by sweeping the trough barriers inwards at a rate of 2.55 mm/min from an area of 20500 mm^2 to achieve the target mean molecular area of 35 $Å^2$/chain. A freshly cleaved HOPG substrate mounted on the automated dipper and was brought down into contact with the air–water interface, with the substrate oriented nearly parallel to the subphase, at a rate of 6 mm/min. Contact was maintained for 2 min before withdrawing the HOPG from the interface at a rate of 6 mm/min. The substrate was then unmounted from the dipper and immediately blown dry with UHP N_2. The TCDA monolayers were then polymerized by UV irradiation (254 nm) for 1 h.

Covalent transfer of striped phase polydiacetylene layers from HOPG to PDMS blends. *Preparation of PDMS coated glass coverslips.* Glass coverslips coated with a thin film of stiff Sylgard-184 PDMS were prepared to support thin samples of soft surface-functionalized custom PDMS blends for transfer and microscopy experiments. Glass coverslips were spin coated using a SPS Polos SPIN 150i spin coater (Putten, Netherlands). Uncured Sylgard-184 (preparation of Sylgard-184 described below) was poured over the coverslips and spun for 30 s at 1000 RPM. The coated glass coverslips were cured over night at 60 °C and stored in closed sample containers under ambient conditions prior to use. *Preparing HOPG substrates for PDMS curing.* To reduce run to run variability in fluorescence measurements, PDMS substrates were prepared with a uniform thickness. TCDA HOPG samples were first covered with 2 cm x 2 cm, 1 mm thick rubber molds (Ted Pella, Inc.) with an 0.5 cm^2 square cut to fit the HOPG area. Double sided clear tape (Scotch brand) was used to create a temporary seal between the HOPG and the rubber mold, preventing leakage of uncured PDMS. *Covalent transfer of PDA films from HOPG to custom PDMS blends.* Custom PDMS blends were prepared in two parts. Part A contained vinyl-terminated polydimethylsiloxane (DMS) base polymer, moderator (1,3,5,7-tetravinyl-1,3,5,7-tetramethylcyclotetrasiloxane), and Pt (Karstedt) catalyst. Part B contained methylhydrosiloxane (HMS) crosslinker and base polymer. The amount of base polymer and crosslinker in the formulation was determined based on desired vinyl:silane stoichiometry as described in the main text. Briefly, each base polymer contains two vinyl groups and a crosslinker contains n Si-H moieties (n_{Si-H}). A 1:1 stoichiometric ratio for n_{Si-H} = 30 will consist of a 15:1 ratio of base polymer:crosslinker. See Supporting information for more detailed experimental protocols including a table of typical reagent amounts utilized for custom PDMS blends.

Unless otherwise stated in the main text, formulations contained 10 ppm catalyst (based on total grams of base polymer), and a 1:2.5 ratio (v/v) of moderator to catalyst. Moderator was added to base polymer in part A and thoroughly mixed before adding the catalyst to ensure a homogeneous distribution of reaction components. Part A and B contained equal amounts of base polymer. For most blends, Part A and B were mixed in a 1:1 ratio (w/w) for 5 min at 400 RPM, then placed in a vacuum chamber for 3 min to remove air bubbles. Degassed mixtures were poured over prepared HOPG substrates and immediately capped with a PDMS coated glass

coverslip. Subsequently, PDMS-coated substrates were cured in an oven at 38 °C for 39 h; the relatively long curing schedule at low temperature was chosen to avoid thermal polymerization of alkydiynes. Exfoliation of the cured PDMS from the HOPG substrates yielded PDMS surfaces of a uniform thickness, covalently linked to the glass coverslip, and functionalized with sPDA; these were stored in closed sample holders under ambient conditions prior to fluorescence characterization.

Covalent transfer of PDA films from HOPG to Sylgard-184. Transfer of sPDA monolayers from HOPG to PDMS was performed using minor modifications of a protocol we developed previously for transfer of sPDA striped phases.[14] Sylgard-184 silicone base and crosslinker (curing agent) were mixed in a 10:1 (w/w) ratio. The mixture was stirred for 10 min at 200 RPM to maximize homogeneity in distribution of the components, followed by degassing in a vacuum chamber for 30 min to remove bubbles. Sylgard-184 was poured on the prepared HOPG surfaces, cured in an oven at 38 °C for 39 h, exfoliated, and stored as described above for custom PDMS blends.

PDMS curing kinetics calculations. PDMS curing kinetics have been examined previously by others,[44-46] typically using the phenomenological Kamal model,[34] which has been established to provide accurate predictions of crosslinking in the early stages of curing.[44] The Kamal autocatalytic model fits the PDMS crosslinking reaction as a function of temperature (T) and conversion to polymer (α), as:

$$\frac{d\alpha}{dt} = (K_1 + K_2\alpha^m)(1-\alpha)^n \qquad (2)$$

where K_1 and K_2 are Arrhenius rate constants ($K_1 = A_1\exp(-E_1/RT)$, $K_2 = A_2\exp(-E_2/RT)$). A recent study[45] used calorimetric analysis of Sylgard-184 to establish Kamal model values of: $E_1 = E_2 = 93.5$ kJ/mol; $A_1 = 7.2 * 10^{10}\ s^{-1}$; $A_2 = 2.9 * 10^{11}\ s^{-1}$; m = 1.04; n = 0.96. At the curing temperature of 38 °C used here, the Kamal model values for Sylgard-184 would lead to calculated values $K_1 = 1.4 * 10^{-5}\ s^{-1}$ and $K_2 = 5.7 * 10^{-5}\ s^{-1}$.

Atomic force microscopy (AFM) imaging. A Veeco MultiMode with a Nanoscope V controller was used to acquire AFM images in tapping mode, using Bruker RFESP-75 tips (nominal force constant 3 N/m and radius of curvature <12 nm) in an ambient environment.

Confocal fluorescence microscopy and spectral imaging. Fluorescence images and emission spectra were acquired using a Zeiss LSM 880 Axio Examiner upright confocal microscope, under the excitation of a 488-nm Ar laser at 100% power, focused through a 20x objective (W Plan-apochromatic 20x/DIC (UV) VIS-IR M27 75 mm). Emitted fluorescence was detected by a 32-channel GaAsP spectral photomultiplier detector with a pinhole size set to 1 Airy unit. All fluorescence images and corresponding spectra were collected at a resolution of 512 x 512 pixels with 8-bit depth. Unidirectional horizontal scans were averaged 16 times/line with a dwell time of 4.10 µs/pixel. Emission spectra were collected from 495–691 nm with a bin width of 8.9 nm.

ASSOCIATED CONTENT

Supporting Information

This material is available free of charge via the Internet at http://pubs.acs.org. Detailed materials and experimental methods, larger AFM and SEM images of TCDA monolayers on HOPG, larger fluorescence images of TCDA monolayers transferred to PDMS, data analysis of confocal fluorescence micrographs, detailed discussion of PDMS transfer probability calculations.

AUTHOR INFORMATION

Corresponding Author

*Address correspondence to: claridge@purdue.edu

Author Contributions

Notes

The authors declare no competing financial interests.

ACKNOWLEDGMENT

SAC acknowledges support through an NSF grant, NSF-CHE-MSN 2108966. Instrumentation in the Purdue Imaging Facility was utilized for optical microscopy experiments.

REFERENCES

1. Xia, Y. N.; Whitesides, G. M. Soft Lithography. *Annu. Rev. Mater. Sci.* **1998,** *28*, 153-184.
2. Whitesides, G. M. Soft Robotics. *Angew. Chem., Int. Ed.* **2018,** *57*, 4258-4273.
3. Heikenfeld, J.; Jajack, A.; Rogers, J. A.; Gutruf, P.; Tian, L.; Pan, T.; Li, R.; Khine, M.; Kim, J.; Wang, J.; Kim, J. Wearable Sensors: Modalities, Challenges, and Prospects. *Lab Chip* **2018,** *18*, 217-248.
4. Bian, P.; Wang, Y.; McCarthy, T. J. Rediscovering Silicones: The Anomalous Water Permeability of "Hydrophobic" PDMS Suggests Nanostructure and Applications in Water Purification and Anti-Icing. *Macromol. Rapid Commun.* **2021,** *42*, 2000682.
5. Wang, L.; McCarthy, M. J. Covalently Attached Liquids: Instant Omniphobic Surfaces with Unprecedented Repellency. *Angew. Chem., Int. Ed.* **2016,** *55*, 244-248.
6. Ray, T. R.; Choi, J. J.; Bandodkar, A. J.; Krishnan, S.; Gutruf, P.; Tian, L.; Ghaffari, R.; Rogers, J. A. Bio-Integrated Wearable Systems: A Comprehensive Review. *Chem. Rev.* **2019,** *119*, 5461-5533.
7. Engler, A.; Backakova, L.; Newman, C.; Hategan, A.; Griffin, M.; Discher, D. Substrate Compliance Versus Ligand Density in Cell on Gel Responses. *Biophys. J.* **2004,** *86*, 617-628.
8. Engler, A. J.; Sen, S.; Sweeney, H. L.; Discher, D. E. Matrix Elasticity Directs Stem Cell Lineage Specification. *Cell* **2006,** *126*, 677-689.
9. Bates, F. S. Polymer-Polymer Phase-Behavior. *Science* **1991,** *251*, 898-905.
10. Bates, F. S.; Hillmyer, M. A.; Lodge, T. P.; Bates, C. M.; Delaney, K. T.; Fredrickson, G. H. Multiblock Polymers: Panacea or Pandora's Box? *Science* **2012,** *336*, 434-440.
11. Zheng, P.; McCarthy, T. J. D_4^h/D_4^v Silicone: A Replica Material with Several Advantages for Nanoimprint Lithography and Capillary Force Lithography. *Langmuir* **2011,** *27*, 7976-7979.
12. Li, Y.; Choi, J.; Sun, Z.; Russell, T. P.; Carter, K. R. Fabrication of Sub-20 nm Patterns Using Dopamine Chemistry in Self-Aligned Double Patterning. *Nanoscale* **2018,** *10*, 20779-20784.
13. Davis, T. C.; Bechtold, J. O.; Shi, A.; Lang, E. N.; Singh, A.; Claridge, S. A. One Nanometer Wide Functional Patterns with a Sub-10 Nanometer Pitch Transferred to an Amorphous Elastomeric Material. *ACS Nano* **2021,** *15*, 1426-1435.
14. Shi, A.; Villarreal, T. A.; Singh, A.; Hayes, T. R.; Davis, T. C.; Brooks, J. T.; Claridge, S. A. Plenty of Room at the Top: A Multi-Scale Understanding of nm-Resolution Polymer Patterning on 2D Materials. *Angew. Chem., Int. Ed.* **2021,** *60*, 25436-25444.

15. Bechtold, J. O.; Arango, J. C.; Shi, A.; Singh, A.; Claridge, S. A. Striped Poly(Diacetylene) Monolayers Control Adsorption of Polyelectrolytes and Proteins on 2D Materials and Elastomers. *ACS Appl. Nano Mater.* **2021,** *4*, 7037-7046.
16. Shi, A.; Singh, A.; Williams, L. O.; Arango, J. C.; Claridge, S. A. Nanometer-Scale Precision Polymer Patterning of PDMS: Multiscale Insights into Patterning Efficiency Using Alkyldiynamines. *ACS Appl. Mater. Interf.* **2022,** *14*, 22634-22642.
17. Arango, J. C.; Williams, L. O.; Shi, A.; Singh, A.; Nava, E. K.; Fisher, R. V.; Garfield, J. A.; Claridge, S. A. Nanostructured Surface Functionalization of Polyacrylamide Hydrogels Below the Length Scale of Hydrogel Heterogeneity. *ACS Appl. Mater. Interf.* **2022,** *14*, 43937-43945.
18. Singh, A.; Arango, J. C.; Shi, A.; d'Aliberti, J. B.; Claridge, S. A. Surface-Templated Glycopolymer Nanopatterns Transferred to Hydrogels for Designed Multivalent Carbohydrate–Lectin Interactions across Length Scales. *J. Am. Chem. Soc.* **2023,** *ASAP. DOI: 10.1021/jacs.2c09937.*
19. Okawa, Y.; Aono, M. Linear Chain Polymerization Initiated by a Scanning Tunneling Microscope Tip at Designated Positions. *J. Chem. Phys.* **2001,** *115*, 2317-2322.
20. Okawa, Y.; Mandal, S. K.; Hu, C.; Tateyama, Y.; Goedecker, S.; Tsukamoto, S.; Hasegawa, T.; Gimzewski, J. K.; Aono, M. Chemical Wiring and Soldering toward All-Molecule Electronic Circuitry. *J. Am. Chem. Soc.* **2011,** *133*, 8227-8233.
21. Shi, A.; Claridge, S. A. Lipids: An Atomic Toolkit for the Endless Frontier. *ACS Nano* **2021,** *15*, 15429-15445.
22. Bang, J. J.; Rupp, K. K.; Russell, S. R.; Choong, S. W.; Claridge, S. A. Sitting Phases of Polymerizable Amphiphiles for Controlled Functionalization of Layered Materials. *J. Am. Chem. Soc* **2016,** *138*, 4448-4457.
23. Rabe, J. P.; Buchholz, S. Commensurability and Mobility in 2-Dimensional Molecular Patterns on Graphite. *Science* **1991,** *253*, 424-427.
24. Schonherr, H.; Feng, C.; Shovsky, A. Interfacial Reactions in Confinement: Kinetics and Temperature Dependence of Reactions in Self-Assembled Monolayers Compared to Ultrathin Polymer Films. *Langmuir* **2003,** *1*, 10843-10851.
25. Feng, C. L.; Vancso, G. J.; Schonherr, H. Interfacial Reactions in Confinement: Kinetics and Temperature Dependence of the Surface Hydrolysis of Polystyrene-Block-Poly(Tert-Butyl Acrylate) Thin Films. *Langmuir* **2005,** *21*, 2356-2363.
26. Jeong, G.; Yu, D. M.; Mapas, J. K. D.; Sun, Z.; Rzayev, J.; Russell, T. P. Realizing 5.4 nm Full Pitch Lamellar Microdomains by a Solid-State Transformation. *Macromolecules* **2017,** *50*, 7148-7154.
27. Yu, D. M.; Mapas, J. K. D.; Kim, H.; Choi, J.; Ribbe, A. E.; Rzayev, J.; Russell, T. P. Evaluation of the Interaction Parameter for Poly(Solketal Methacrylate)-Block-Polystyrene Copolymers. *Macromolecules* **2018,** *51*, 1031-1040.
28. Ortiz-Acosta, D.; Densmore, C. *Sylgard Cure Inhibition Characterization*; Los Alamos National Laboratory: 2012.
29. Florke, O. W.; Graetsch, H. A.; Brunk, F.; Brenda, L.; Paschen, S.; Bergna, H. E.; Roberts, W. O.; Welsh, W. A.; Libanati, C.; Ettlinger, M.; Kerner, D.; Maier, M.; Meon, W.; Schmoll, R.; Gies, H.; Schiffmann, D., Silica. In *Ullmann's Encyclopedia of Industrial Chemistry*, Wiley-VCH Verlag: Weinheim, 2012; Vol. 32, pp 421-507.
30. Cyr, D. M.; Venkataraman, B.; Flynn, G. W. STM Investigations of Organic Molecules Physisorbed at the Liquid-Solid Interface. *Chem. Mater.* **1996,** *8*, 1600-1615.
31. De Feyter, S.; De Schryver, F. C. Two-Dimensional Supramolecular Self-Assembly Probed by Scanning Tunneling Microscopy. *Chem. Soc. Rev.* **2003,** *32*, 139-150.
32. Lécuiller, R.; Berréhar, J.; Lapersonne-Meyer, C.; Schott, M. Dual Resonance Fluorescence of Polydiacetylene Chains Isolated in Their Crystalline Monomer Matrix. *Phys. Rev. Lett.* **1998,** *80*, 4068-4071.
33. Lewis, L. N.; Stein, J.; Gao, Y.; Colborn, R. E.; Hutchins, G. Platinum Catalysts Used in the Silicones Industry. *Platinum Met. Rev.* **1997,** *41*, 66-75.
34. Kamal, M. R.; Sourour, S. Kinetics and Thermal Characterization of Thermoset Cure. *Polym. Eng. Sci.* **1973,** *13*, 59-64.
35. Meissner, B.; Matejka, L. Kinetic Limitation in the Formation of End-Linked Elastomer Networks. *Polymer* **2005,** *46*, 10618-10625.
36. Porter, A. G.; Ouyang, T.; Hayes, T. R.; Biechele-Speziale, J.; Russell, S. R.; Claridge, S. A. 1-nm-Wide Hydrated Dipole Arrays Regulate AuNW Assembly on Striped Monolayers in Nonpolar Solvent. *Chem* **2019,** *5*, 2264-2275.
37. Lang, E. N.; Porter, A. G.; Ouyang, T.; Shi, A.; Hayes, T. R.; Davis, T. C.; Claridge, S. A. Oleylamine Impurities Regulate Temperature-Dependent Hierarchical Assembly of Ultranarrow Gold Nanowires on Biotemplated Interfaces. *ACS Nano* **2021,** *15*, 10275-10285.
38. Lang, E. N.; Pintro, C.; Claridge, S. A. Trans and Saturated Alkyl Impurities in Technical-Grade Oleylamine: Limited Miscibility and Impacts on Nanocrystal Growth *Chem. Mater.* **2022,** *34*, 5273-5282.
39. Butts, M.; Cella, J.; Wood, C. D.; Gillette, G.; Kerboua, R.; Leman, J.; Lewis, L.; Rubinsztajn, S.; Schattenmann, F.; Stein, J.; Wicht, D.; Rajaraman, S.; Wengrovius, J., Silicones. In *Kirk-Othmer Encyclopedia of Chemical Technology*, Wiley & Sons: New York, 2006; Vol. 22.
40. Bang, J. J.; Rupp, K. K.; Russell, S. R.; Choong, S. W.; Claridge, S. A. Sitting Phases of Polymerizable Amphiphiles for Controlled Functionalization of Layered Materials. *J. Am. Chem. Soc.* **2016,** *138*, 4448-4457.
41. Davis, T. C.; Bang, J. J.; Brooks, J. T.; McMillan, D. G.; Claridge, S. A. Hierarchically Patterned Noncovalent Functionalization of 2D Materials by Controlled Langmuir-Schaefer Conversion. *Langmuir* **2018,** *34*, 1353-1362.
42. Bang, J. J.; Porter, A. G.; Davis, T. C.; Hayes, T. R.; Claridge, S. A. Spatially Controlled Noncovalent Functionalization of 2D Materials Based on Molecular Architecture. *Langmuir* **2018,** *34*, 5454-5463.
43. Hayes, T. R.; Bang, J. J.; Davis, T. C.; Peterson, C. F.; McMillan, D. G.; Claridge, S. A. Multimicrometer Noncovalent Monolayer Domains on Layered Materials through Thermally Controlled Langmuir-Schaefer Conversion for Noncovalent 2D Functionalization. *ACS Appl. Mater. Interf.* **2017,** *9*, 36409–36416.
44. Harkous, A.; Colomines, G.; Leroy, E.; Mousseau, P.; Deterre, R. The Kinetic Behavior of Liquid Silicone Rubber: A Comparison between Thermal and Rheological Approaches Based on Gel Point Determination. *React. Funct. Polym.* **2016,** *101*, 20-27.
45. Bardelli, T.; Marano, C.; Vangosa, F. B. Polydimethylsiloxane Crosslinking Kinetics: A Systematic Study on Sylgard184 Comparing Rheological and Thermal Approaches. *J. Appl. Polym. Sci.* **2021,** *138*, e51013.
46. Lopez, L. M.; Cosgrove, A. B.; Hernandez-Ortiz, J. P.; Osswald, T. A. Modeling the Vulcanization Reaction of Silicone Rubber. *Polym. Eng. Sci.* **2007**, 675-683.

TABLE OF CONTENTS GRAPHIC: